Coherent Diffraction Radiation of Relativistic Terahertz Pulses from a Laser-Driven Microplasma Waveguide

Longqing Yi* and Tünde Fülöp
Department of Physics, Chalmers University of Technology, 41296 Gothenburg, Sweden

(Received 18 April 2019; published 27 August 2019)

We propose a method to generate isolated relativistic terahertz (THz) pulses using a high-power laser irradiating a microplasma waveguide (MPW). When the laser pulse enters the MPW, high-charge electron bunches are produced and accelerated to ∼100 MeV by the transverse magnetic modes. A substantial part of the electron energy is transferred to THz emission through coherent diffraction radiation as the electron bunches exit the MPW. We demonstrate this process with three-dimensional particle-in-cell simulations. The frequency of the radiation is determined by the incident laser duration, and the radiated energy is found to be strongly correlated to the charge of the electron bunches, which can be controlled by the laser intensity and microengineering of the MPW target. Our simulations indicate that 100 mJ level relativistic-intense THz pulses with tunable frequency can be generated at existing laser facilities, and the overall efficiency reaches 1%.

DOI: 10.1103/PhysRevLett.123.094801

High power terahertz (THz) pulses have attracted significant attention since they can serve as a unique and versatile tool in fields ranging from biological imaging to material science [1–4]. In particular, at high intensities, such pulses allow manipulation of the transient states of matter, for example, giving control over the electronic, spin, and ionic degrees of freedom of molecules and solids [5]. Several methods such as two-color laser filamentation [6], optical rectification in lithium-niobate [7,8] or organic crystals [9], and relativistic laser irradiated plasmas [10–18], have been developed for generation of THz pulses with electric fields above 1 MV/cm. However, scaling up such methods towards higher intensities remains challenging, thus representing an active research field.

Relativistic electron beams have also been used to produce THz radiation through a variety of mechanisms that include synchrotron radiation [19], transition radiation [20,21], and diffraction radiation [22,23]. Radiation emitted by these mechanisms is coherent if the bunch length is shorter than the radiated wavelength of interest. The radiated energy then scales as the square of the beam charge. Previous studies have also shown that the radiation power decreases significantly with the beam divergence, and the energy radiated in a small cone near axis would strongly benefit from a high beam energy [24]. Therefore, choosing an electron source with desired qualities (high charge, high energy, and well-collimated) can be crucial for producing intense THz emission that is attractive for a range of applications [5].

Currently available sources of relativistic electron beams are either linear accelerators or compact sources based on laser-plasma acceleration. The THz radiation energy from linear accelerators has reached ∼600 μJ/pulse [25], but such sources are expensive and large and thus can only offer limited accessibility. Laser wakefield acceleration in the nonlinear "bubble" regime can produce multi-GeV electron beams with small divergence (∼0.1 mrad), but only small charge (1–100 pC) [26]. Self-modulated laser-wakefield acceleration can produce nano-Coulomb (nC) electron bunches [27] but typically have a temperature of a few MeVs, and the beam divergence is large due to direct laser acceleration [28]. Hot electrons that arise from laser-solid interaction can reach up to nC-μC charge, but the temperature is typically only a few hundreds of keVs to a few MeVs, and the divergence is usually large (∼40°) [13]. Recently, THz radiation energy above the millijoule (mJ) level has been reported in laser-solid interaction [17], but since a picosecond laser pulse is used, the coherent frequency range is below 1 THz, and the efficiency is ∼0.1%.

In this Letter, we propose a scheme to efficiently generate isolated THz pulses with electric fields beyond 1 GV/cm. As illustrated in Fig. 1(a), an intense laser pulse is focused into a microplasma waveguide (MPW), leading to electrons being extracted from the wall and accelerated by longitudinal electric fields of the transverse magnetic modes up to a few hundreds of MeVs [29–33]. The divergence is usually a few degrees and the duration is the same as the laser pulse. Typically, the electron beam inherits the density of the plasma skin layer ($n_{\mathrm{beam}} \sim n_c$, where $n_c = m_e\omega_0^2/4\pi e^2$ is the critical density, e and m_e are the elementary charge and the electron mass, ω_0 is the laser frequency) from which it is generated [34]. Thus, a total charge of a few tens of nC can be obtained with 100-fs high-power laser systems. Recently, this idea has been demonstrated experimentally with a laser interacting with a microchannel plate [35]. Such an electron source is suitable

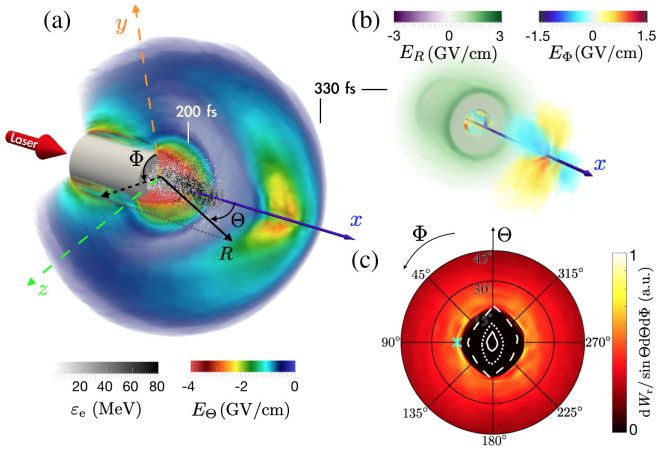

FIG. 1. (a) Schematics of the proposed setup. A laser pulse is focused on the entrance of a MPW (white cylinder), which produces electrons and accelerates them up to ~100 MeV. As the electron beam (black-white dots, the color represents their energy) exits the MPW (200 fs), THz emission is generated by CDR. E_Θ field at 200 and 330 fs is shown in (a), where a quarter is removed to show the color scale inside the radiation shell. (b) E_R and E_Φ components at 330 fs. The angular distribution of the radiated THz energy at 330 fs within $\Theta < 45°$ is presented in (c). The white dashed, dotted, and solid lines in (c) are contours of electron beam density at 0.1, 0.4, and 0.7 of the maximum density, respectively. The density contours in (c) are taken at 200 fs when the beam just leaves the MPW, and the cyan cross marks the observation angle in Fig. 2.

for THz generation based on coherent transition radiation and/or coherent diffraction radiation (CDR).

The MPW target we consider is a small channel of a few microns in diameter in glass or plastic material, being widely available as a standard microchannel plate used for x-ray detection [36]. It is different from the plasma channel produced by an intense laser pulse in a gas target [37], which is also proposed for THz generation [38]. The scheme proposed here takes advantage of unique features of electron beam generation in MPW, such as beam size comparable to the laser pulse length and absence of the beam loading effect [39]. This leads to the production of easily tunable (from sub-THz to infrared) pulses with a high conversion efficiency (~1%) that can be maintained when scaling towards higher intensities, allowing for achieving multi-hundreds-mJ THz energy.

We demonstrate our scheme using three-dimensional (3D) particle-in-cell (PIC) simulations with the EPOCH code [40]. A linearly polarized (in the y direction) laser with intensity 1.4×10^{20} W/cm^2 (normalized intensity $a_0 = eE_0/m_e c\omega_0 = 10$, where E_0 is the amplitude of the laser electric field and c is the speed of light) is focused on the entrance of a MPW, propagating along the x axis. The laser beam has a temporal Gaussian profile with FWHM duration of $\tau_0 = 54$ fs and a focal spot $w_0 = 4\lambda_0$, where $\lambda_0 = 1$ μm is the laser wavelength. The MPW is modeled with a pre-ionized cylindrical plasma channel, with maximum density of $n_0 = 15n_c$, the inner and outer radii are $r_0 = 5$ and $r_1 = 10$ μm, respectively. The longitudinal length of the MPW is $L = 30$ μm. Because of the heating of the laser prepulse, the inner surface ($r < r_0$, where $r = \sqrt{y^2 + z^2}$) is assumed to have a density gradient $n(r) = n_0 \exp[-(r - r_0)^2/\sigma_0^2]$, and the scale length is $\sigma_0 = 1$ μm. This leads to an effective radius $r_c = 3.35$ μm, where $n(r_c) = 1n_c$. It should be noted that although the maximum density n_0 must be limited for computational efficiency, it makes little difference in the results since the laser can hardly penetrate into the area with $n > 15n_c$ due to the finite density gradient. This is confirmed by 2D simulations with maximum density $n_0 = 100n_c$. The dimensions of the simulation box are $x \times y \times z = 100 \times 80 \times 80$ μm and are sampled by $2500 \times 800 \times 800$ cells with 8 macroparticles for electrons and 2 for C^{6+} ions (the particles are created with different weights corresponding to the initial local density). The algorithm proposed by Cowan *et al.* [41] is used to minimize the numerical dispersion.

The electric fields in the simulation with frequency below 60 THz are presented in Figs. 1(a)–1(b), where a 35-mJ THz pulse is obtained, and the radiated power reaches 0.7 TW (calculated at 330 fs and for the region $x > 41$ μm). To show the polarisation of the CDR, we apply spherical coordinates with the origin at the exit of MPW on the laser propagation axis $x_c = 31$ μm, and convert the coordinates according to $R = \sqrt{(x - x_c)^2 + y^2 + z^2}$, $\Theta = \arcsin(r/R)$, and $\Phi = \arctan(z/y)$ as illustrated in Fig. 1(a).

The radiation fields are emitted simultaneously with electron propagation through the aperture at $x = x_c$, mostly confined in a spherical shell. The THz emission is predominantly radially polarized in the plane determined by the observation line of sight and the laser propagation axis. The polar component, E_Θ, contains 99% of the radiation energy. The preference of electron distribution in the laser polarization direction results in a small quadrupolar azimuthal electric field E_Φ. The radial component E_R is negligible in the radiating shell.

The angular distribution of THz energy in the forward direction is shown in Fig. 1(c), with white lines in the centre representing the electron beam density. The electrons reach a cutoff energy of 100 MeV, and their total charge is 7.4 nC. The divergence of the electron beam is about 10°. A depleted area is observed within the electron beam, because the radiation fields add coherently and tend to cancel each other in this region. Since the electron energy is high, the CDR power is strongly peaked on the edge of the beam [42]. The intensity rises sharply forming a very thin layer ($\Delta\Theta \sim 1°$) around $\Theta \sim 17°$. The electron beam is slightly elongated along the laser polarization direction, which leads to a higher radiation power in the direction perpendicular to it.

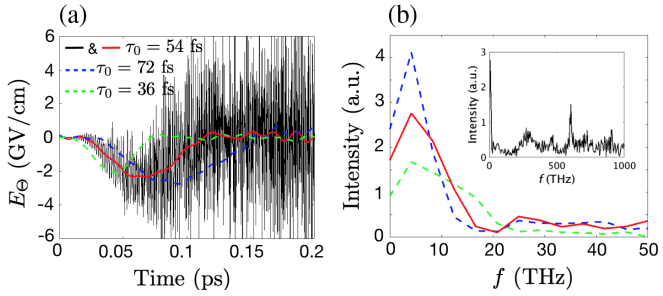

FIG. 2. The radiation fields E_Θ (a) and their spectra (b) observed at $\Theta = 17°$ and $\Phi = 90°$, the black and red lines represent the CDR with and without a low-pass filter (frequency below 60 THz) for laser FWHM duration $\tau_0 = 54$ fs. The green and blue dashed lines show the cases driven by τ_0 equals to 36 and 72 fs, respectively. The inset in (b) is the full-spectrum (0–1000 THz) for $\tau_0 = 54$ fs.

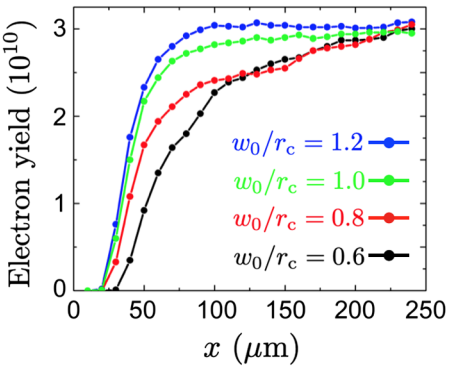

FIG. 3. The electron yield vs propagation distance, for different w_0/r_c ratios.

The radiation field seen at $\Theta = 17°$, $\Phi = 90°$ is shown by the black line in Fig. 2(a). The red line shows the low-frequency component below 60 THz. The amplitude of the half-cycle THz pulse is 3 GV/cm, corresponding to a normalised amplitude of $a_{\mathrm{THz}} = 1.6$, reaching the relativistic intensity. Figure 2(b) shows the spectra of the radiation fields: most of the pulse energy concentrates in the desired THz frequency range of 1–10 THz. The inset in Fig. 2(b) shows the spectrum from 0 to 1000 THz for $\tau_0 = 54$ fs, with a small bump around the laser frequency at 300 THz and a peak at the double frequency 600 THz. The latter is the result of the modulation of the electron beam at $2\omega_0$, and can serve as an experimental signature of the CDR [24].

In Fig. 2 the green and blue dashed lines represent the radiation field (after frequency filtering) and spectra produced by laser pulses with τ_0 of 36 and 72 fs, respectively. The radiated frequency is determined by the duration of electron beam, which coincides with the laser pulse. With currently available laser systems, this scheme is capable of generating relativistic pulses with frequencies ranging from infrared to sub-THz.

The mechanism of the electron beam generation, i.e., the electrons injected into the channel (vacuum core of the MPW), is crucial for understanding the THz radiation power. The production of electron bunches at a plasma-vacuum interface can be attributed to the counterstreaming electrons percolating through the laser nodes, as the laser pushes the surface electrons inwards [34]. In the MPW, the underlying physics is similar, but the mechanism that pushes the surface electrons, and the associated counterstreaming, depends on the ratio of the laser focal spot size (w_0) and the effective MPW radius (r_c).

To show this, we perform 2D PIC simulations of lasers having different focal spot sizes propagating in a long waveguide (240 μm). The laser and plasma parameters are the same as in the 3D simulation unless otherwise described. The resolution is 50 and 20 cells per laser wavelength in longitudinal and transverse directions, respectively. The third dimension is assumed to be 4 μm when estimating the electron number. In Fig. 3, we plot the total electron number (above 10 MeV) against the propagation distance for different w_0/r_c ratios (the laser energy is fixed).

Figure 3 shows that when $w_0/r_c \geq 1$, the injection occurs rapidly at the entrance of the MPW. This is because the initial impact of the laser and MPW front surface is violent, which leads to strong diffracted light that results in significant counterstreaming. The electrons are more likely to be injected at this stage. In the cases where $w_0/r_c < 1$, the injection at the entrance is reduced and the injection inside the MPW becomes important, which is due to the interaction between waveguide modes and the MPW wall. The photon momentum $\hbar k_T$, associated with the transverse wave number k_T, pushes the surface plasma radially as the light is bouncing between the walls.

Interestingly, despite different injection processes, all cases result in similar beam charges for sufficiently long MPW. This is because in order to be injected into the channel, the electrons percolating through the laser nodes must overcome the electrostatic potential barrier near the MPW wall, which leads to saturation. The charge injected at the entrance suppresses the injection inside the channel. In the end, the maximum charge separation on the wall will be just sufficient to prevent the most energetic counterstreaming electrons inside the MPW from escaping. The energy of these electrons is determined by the fundamental waveguide mode.

To estimate the energy of the electrons we use momentum conservation. Note that the ion response time is typically longer than the interaction timescale. The number of plasma electrons streaming towards the MPW inner surface (counterstream due to charge separation) per unit time is $N_e \approx n_c \pi r_c^2 \beta' c k_x / k_T$, where k_T and k_x are the transverse and longitudinal wave number in the MPW, β' is the radial velocity of counterstreaming electrons normalised by c. These electrons are reflected back on the plasma-vacuum interface due to the interaction with the

photons (N_γ per unit time). We assume the number of electrons percolating through the laser nodes as well as the number of the photons absorbed are negligibly small. According to momentum conservation $2N_\gamma \hbar k_T = N_e(\gamma\beta_r + \gamma'\beta')m_e c$, where $\gamma' = (1-\beta'^2)^{-1}$, γ and β_r are the relativistic gamma factor and the normalised radial velocity of the electrons that are pushed inwards.

Here we are only interested in the maximum counterstreaming electron energy that can be achieved. Substituting $\beta_r \approx \beta'$ due to quasineutrality, we find that γ' reaches its maximum when $\gamma \approx \gamma'$ is satisfied (i.e., the surface electrons are pushed primarily in the radial direction),

$$\gamma'_{\max} \approx \frac{\Gamma + \sqrt{\Gamma^2 + 4}}{2}, \tag{1}$$

where $\Gamma \equiv (x_1^2 a_m^2)/(k_0^2 r_c^2)$, $k_0 = \sqrt{k_x^2 + k_T^2}$, and a_m is the normalized intensity of the waveguide mode. For $w_0 \geq r_c$, $a_m \approx a_0$, and for $w_0 < r_c$, $a_m = a_0 w_0/r_c$. We have assumed the radius of MPW is sufficiently large ($k_T \ll k_0$), and only the fundamental mode exists inside the MPW, so that $k_T = x_1/r_c$ and $x_1 \approx 2.4$ is the first root of the eigenvalue equation [43].

The electrostatic field near the MPW wall can be estimated using Gauss's law, $E_C = 2Q/r_c c\tau_0$, where Q is the charge that is lost from the wall (i.e., injected into the channel). Further injection can only happen when the kinetic energy of counterstreaming electrons overcomes the electrostatic potential within the skin layer, i.e., $(\gamma'_{\max} - 1)m_e c^2 \approx \sqrt{\gamma'_{\max}} e E_C c/\omega_0$, which yields the saturation charge,

$$Q \approx \frac{(\gamma'_{\max} - 1)}{\sqrt{\gamma'_{\max}}} \frac{k_0 r_c}{2} \frac{m_e c^3}{e} \tau_0. \tag{2}$$

As an order-of-magnitude estimate, for a microsized channel, $k_0 r_c$ is typically around unity. This means that a 10^{20} W/cm^2, 50-fs laser system could produce 10 nC electron beams, which agrees with simulations. From Eq. (2) the scaling of the charge with the normalized laser intensity can be estimated: for weakly relativistic cases ($\Gamma \ll 1$) $Q \propto a_m^2/r_c$, while for strongly relativistic cases ($\Gamma \gg 1$) $Q \propto a_m$. Note, that the energy of CDR scales as $W_r \propto Q^2$; it is therefore important to confirm these scalings by 3D PIC simulations to guide future experiments.

In Fig. 4(a), we plot the electron charge produced by the MPW and the total THz energy (below 60 THz) as functions of a_0, where $r_c = 3.35$ and $w_0 = 4$ μm are fixed, and the MPW length is $L = 30$ μm. The parameters are the same as in Fig. 1 unless otherwise stated. It is shown that the charge increases quadratically with the laser intensity ($Q \propto a_0^2$) when a_0 is small, and the scaling becomes linear ($Q \propto a_0$) for $a_0 > 8$, where Γ exceeds unity. In addition, the simulation results indicate that the THz energy can be fitted by $W_r \propto a_0^4$ in the weakly relativistic regime, where the conversion efficiency increases with the intensity. In the strongly relativistic regime, the THz energy can be fitted by $W_r \propto a_0^2$ and the conversion efficiency is maintained at ~1%. These results also demonstrate that the radiation is coherent ($W_r \propto Q^2$). Our simulations suggest that TW class, 100-mJ strong THz emission can be produced by a 10 J/250 TW laser system, which is within reach of the existing laser facilities.

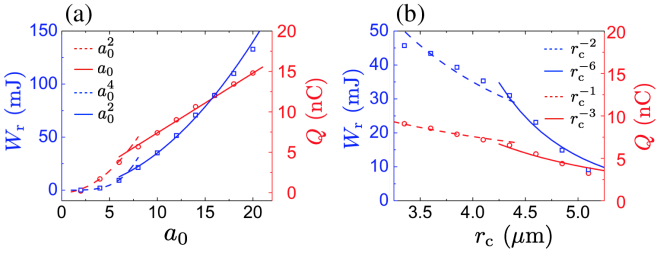

FIG. 4. The electron beam charge (red) and the THz radiation energy (blue) evolution with varying (a) laser intensity and (b) effective MPW radii. Open markers are 3D PIC simulation results (circles and squares represent the electron charge and THz energy respectively), and the solid and dashed curves are fittings suggested by Eq. (2).

In Fig. 4(b), we consider the effects of varying the MPW radius when the laser parameters are fixed ($a_0 = 10$ and $w_0 = 4$ μm), and the MPW length is extended to $L = 120$ μm to ensure sufficient distance for injection. In this case, Eq. (2) leads to $Q \propto r_c^{-1}$ in the strongly relativistic regime, and $Q \propto r_c^{-3}$ in the weakly relativistic regime, which agrees with our simulations. Since the radiation is coherent, it results in a quenching effect: the radiation energy drops dramatically ($W_r \propto r_c^{-6}$) as the effective radius exceeds a threshold near $\Gamma \sim 1$. This is verified by a sharp decrease of the THz energy at the separatrix of the two regimes around $r_c \approx 4.3$ μm ($\Gamma \approx 0.7$).

Finally, we note that Eq. (2) does not consider the effects of high-order waveguide modes and strong diffraction at the entrance, both effects give a higher transverse light pressure. In fact, the value from Eq. (2) should be treated as the minimum charge that can be produced by laser-MPW interaction, as the interaction between the lowest-order mode and MPW is the weakest. A detailed study of these effects is left for future work.

In conclusion, we proposed a scheme to generate relativistic isolated THz pulses based on the interaction of a laser pulse with a microplasma waveguide. 3D PIC simulations show that an energetic electron beam with a few tens of nC charge can be produced. As the beam exits the waveguide, a substantial part of the electron energy is transferred to an intense THz emission through coherent diffraction radiation. We demonstrated that the overall efficiency reaches 1%, the radiation power 1 TW and the energy 100 mJ. The proposed scheme can be easily

extended to other frequency ranges by varying the driving laser duration, allowing the generation of radiation from infrared to sub-THz range with relativistic intensities. This opens a new avenue towards high-power light matter interaction beyond the state of the art.

The authors acknowledge fruitful discussions with I. Thiele, S. Newton, I. Pusztai, E. Siminos, and J. Ferri. This work is supported by the Olle Engqvist Foundation, the Knut and Alice Wallenberg Foundation, and the European Research Council (ERC-2014-CoG Grant No. 647121). Simulations were performed on resources at Chalmers Centre for Computational Science and Engineering (C3SE) provided by the Swedish National Infrastructure for Computing (SNIC).

*longqing@chalmers.se

[1] M. Tonouchi, Nat. Photonics **1**, 97 (2007).
[2] P. H. Siegel, IEEE Trans. Microwave Theory Tech. **52**, 2438 (2004).
[3] B. E. Cole, J. B. Williams, B. T. King, M. S. Shervin, and C. R. Stanley, Nature (London) **410**, 60 (2001).
[4] M. C. Hoffmann and J. A. Fülöp, J. Phys. D **44**, 083001 (2011).
[5] T. Kampfrath, K. Tanaka, and K. Nelson, Nat. Photonics **7**, 680 (2013).
[6] T. I. Oh, Y. J. Yoo, Y. S. You, and K. Y. Kim, Appl. Phys. Lett. **105**, 041103 (2014).
[7] H. Hirori, A. Doi, F. Blanchard, and K. Tanaka, Appl. Phys. Lett. **98**, 091106 (2011).
[8] J. A. Fülöp, Z. Ollmann, Cs. Lombosi, C. Skrobol, S. Klingebiel, L. Pálfalvi, F. Krausz, S. Karsch, and J. Hebling, Opt. Express **22**, 20155 (2014).
[9] C. Vicario, B. Monoszlai, and C. P. Hauri, Phys. Rev. Lett. **112**, 213901 (2014).
[10] Z. M. Sheng, K. Mima, J. Zhang, and H. Sanuki, Phys. Rev. Lett. **94**, 095003 (2005).
[11] A. Gopal, S. Herzer, A. Schmidt, P. Singh, A. Reinhard, W. Ziegler, D. Brömmel, A. Karmakar, P. Gibbon, U. Dillner, T. May, H. G. Meyer, and G. G. Paulus, Phys. Rev. Lett. **111**, 074802 (2013).
[12] Y. T. Li, C. Li, M. L. Zhou, W. M. Wang, F. Du, W. J. Ding, X. X. Lin, F. Liu, Z. M. Sheng, X. Y. Peng, L. M. Chen, J. L. Ma, X. Lu, Z. H. Wang, Z. Y. Wei, and J. Zhang, Appl. Phys. Lett. **100**, 254101 (2012).
[13] G. Q. Liao, Y. T. Li, Y. H. Zhang, H. Liu, X. L. Ge, S. Yang, W. Q. Wei, X. H. Yuan, Y. Q. Deng, B. J. Zhu, Z. Zhang, W. M. Wang, Z. M. Sheng, L. M. Chen, X. Lu, J. L. Ma, X. Wang, and J. Zhang, Phys. Rev. Lett. **116**, 205003 (2016).
[14] Y. Tian, J. S. Liu, Y. F. Bai, S. Y. Zhou, H. Y. Sun, W. W. Liu, J. Y. Zhao, R. X. Li, and Zhizhan Xu, Nat. Photonics **11**, 242 (2017).
[15] Z. Y. Chen and A. Pukhov, Phys. Plasmas **22**, 103105 (2015).
[16] S. Herzer, A. Woldegeorgis, J. Polz, A. Reinhard, M. Almassarani, B. Beleites, F. Ronneberger, R. Grosse, G. G. Paulus, U. Hübner, T. May, and A. Gopal, New J. Phys. **20**, 063019 (2018).
[17] G. Q. Liao, Y. T. Li, H. Liu, G. G. Scott, D. Neely, Y. H. Zhang, B. J. Zhu, Z. Zhang, C. Armstrong, E. Zemaityte, P. Bradford, P. G. Huggard, D. R. Rusby, P. McKenna, C. M. Brenner, N. C. Woolsey, W. M. Wang, Z. M. Sheng, and J. Zhang, Proc. Natl. Acad. Sci. U.S.A. **116**, 3994 (2019).
[18] I. Thiele, E. Simios, and T. Fülöp, Phys. Rev. Lett. **122**, 104803 (2019).
[19] G. L. Carr, M. C. Martin, W. R. McKinney, K. Jordan, G. R. Neil, and G. P. Williams, Nature (London) **420**, 153 (2002).
[20] V. L. Ginzburg, Phys. Scr. **T2A**, 182 (1982).
[21] U. Happek, A. J. Sievers, and E. B. Blum, Phys. Rev. Lett. **67**, 2962 (1991).
[22] Yu. N. Dnestrovskii and D. P. Kostomarov, Dokl. Akad. Nauk **124**, 792 (1959) [Sov. Phys. Dokl. **4**, 132 (1959)]; **124**, 1026 (1959) [**4**, 158 (1959)].
[23] Y. Shibata, S. Hasebe, K. Ishi, T. Takahashi, T. Ohsaka, and M. Ikezawa, Phys. Rev. E **52**, 6787 (1995).
[24] C. B. Schroeder, E. Esarey, J. van Tilborg, and W. P. Leemans, Phys. Rev. E **69**, 016501 (2004).
[25] Z. Wu, A. S. Fisher, J. Goodfellow, M. Fushs, D. Darancinang, M. Hogan, H. Loos, and A. Lindenberg, Rev. Sci. Instrum. **84**, 022701 (2013).
[26] W. P. Leemans, A. J. Gonsalves, H. S. Mao, K. Nakamura, C. Benedetti, C. B. Schroeder, C. Tóth, J. Daniels, D. E. Mittelberger, S. S. Bulanov, J. L. Vay, C. G. R. Geddes, and E. Esarey, Phys. Rev. Lett. **113**, 245002 (2014).
[27] W. P. Leemans, P. Catravas, E. Esarey, C. G. R. Geddes, C. Toth, R. Trines, C. B. Schroeder, B. A. Shadwick, J. van Tilborg, and J. Faure, Phys. Rev. Lett. **89**, 174802 (2002).
[28] C. Gahn, G. D. Tsakiris, A. Pukhov, J. Meyer-ter-Vehn, G. Pretzler, P. Thirolf, D. Habs, and K. J. Witte, Phys. Rev. Lett. **83**, 4772 (1999).
[29] S. V. Bulanov, F. F. Kamenets, F. Pegoraro, and A. M. Pukhov, Phys. Lett. A **195**, 84 (1994).
[30] L. Q. Yi, A. Pukhov, P. Luu-Thanh, and B. F. Shen, Phys. Rev. Lett. **116**, 115001 (2016).
[31] L. Q. Yi, A. Pukhov, and B. F. Shen, Phys. Plasmas **23**, 073110 (2016).
[32] L. Q. Yi, A. Pukhov, and B. F. Shen, Sci. Rep. **6**, 28147 (2016).
[33] Z. Gong, A. P. L. Robinson, X. Q. Yan, and A. V. Arefiev, Plasma Phys. Controlled Fusion **61**, 035012 (2019).
[34] N. Naumova, I. Sokolov, J. Nees, A. Maksimchuk, V. Yanovsky, and G. Mourou, Phys. Rev. Lett. **93**, 195003 (2004).
[35] J. Snyder, L. L. Ji, K. M. George, C. Willis, G. E. Cochran, R. L. Daskalova, A. Handler, T. Rubin, P. L. Poole, D. Nasir, A. Zingale, E. Chowdhury, B. F. Shen, and D. W. Schumacher, Phys. Plasmas **26**, 033110 (2019).
[36] T. Gys, Nucl. Instrum. Methods Phys. Res., Sect. A **787**, 254 (2015).
[37] C. G. Durfee III, J. Lynch, and H. M. Milchberg, Phys. Rev. E **51**, 2368 (1995).
[38] J. Déchard, A. Debayle, X. Davoine, L. Gremillet, and L. Bergé, Phys. Rev. Lett. **120**, 144801 (2018).
[39] T. Katsouleas, W. Lu, F. S. Tsung, C. Huang, W. B. Mori, T. Katsouleas, J. Vieira, R. A. Fonseca, and L. O. Silva, Phys. Plasmas **16**, 056705 (2009).

[40] T. D. Arber, K. Bennett, C. S. Brady, A. Lawrence-Douglas, M. G. Ramsay, N. J. Sircombe, P. Gillies, R. G. Evans, H. Schmitz, A. R. Bell, and C. P. Ridgers, Plasma Phys. Controlled Fusion **57**, 113001 (2015).
[41] B. M. Cowan, D. L. Bruhwiler, J. R. Cary, and E. Cormier-Michel, Phys. Rev. Accel. Beams **16**, 041303 (2013).
[42] N. J. Carron, Prog. Electromagn. Res. **28**, 147 (2000).
[43] H. M. Shen, J. Appl. Phys. **69**, 6827 (1991).